

# Effects of quarks on the formation and evolution of $Z(3)$ walls and strings in relativistic heavy-ion collisions

Uma Shankar Gupta<sup>1,\*</sup>, Ranjita K. Mohapatra<sup>2,†</sup>, Ajit M. Srivastava<sup>2,‡</sup> and Vivek K. Tiwari<sup>1,§</sup>

<sup>1</sup>*Physics Department, Allahabad University, Allahabad 211002, India*

<sup>2</sup>*Institute of Physics, Sachivalaya Marg, Bhubaneswer 751005, India*

We investigate the effects of explicit breaking of  $Z(3)$  symmetry due to the presence of dynamical quarks on the formation and evolution of  $Z(3)$  walls and associated QGP strings within Polyakov loop model. We carry out numerical simulations of the first order quark-hadron phase transition via bubble nucleation (which may be appropriate, for example, at finite baryon chemical potential) in the context of relativistic heavy-ion collision experiments. Using appropriate shifting of the order parameter in the Polyakov loop effective potential, we calculate the bubble profiles using bounce technique, for the true vacuum as well as for the metastable  $Z(3)$  vacua, and estimate the associated nucleation probabilities. These different bubbles are then nucleated and evolved and resulting formation and dynamics of  $Z(3)$  walls and QGP strings is studied. We discuss various implications of the existence of these  $Z(3)$  interfaces and the QGP strings, especially in view of the effects of the explicit breaking of the  $Z(3)$  symmetry on the formation and dynamical evolution of these objects.

PACS numbers: 25.75.-q, 12.38.Mh, 11.27.+d

Key words: quark-hadron transition, relativistic heavy-ion collisions,  $Z(3)$  domain walls

## I. INTRODUCTION

The possibility of existence of topologically non-trivial structures such as  $Z(3)$  interfaces and associated QGP strings in the quark-gluon plasma phase [1] is very exciting. In the context of relativistic heavy-ion collision experiments (RHICE), it provides the only system where domain walls and strings arise in a relativistic quantum field theory which can be investigated under laboratory control. In earlier works [1–3] we have discussed various aspects of existence of these objects in cosmology as well as in RHICE. These topological objects arise in the high temperature deconfined phase of QCD due to spontaneous breaking of the  $Z(3)$  global symmetry of finite temperature QCD, where  $Z(3)$  is the center of the  $SU(3)$  color gauge group of QCD. Spontaneous breaking of  $Z(3)$  symmetry arises from the non-zero expectation value of the Polyakov loop,  $l(x)$ , which is an order parameter for the confinement-deconfinement phase transition for pure gauge theory [4]. The interpolation of  $l(x)$  between three different degenerate  $Z(3)$  vacua leads to the existence of domain walls (interfaces) together with topological strings when the three interfaces make a junction. We call these strings as QGP strings [1].

The properties and physical consequences of these  $Z(3)$  interfaces have been discussed in the literature[5]. It has also been suggested that these interfaces should not be taken as physical objects in the Minkowski space [6]. Existence of these  $Z(3)$  vacua becomes especially a non-trivial issue when considering the presence of dynamical quarks. The effect of quarks on  $Z(3)$  symmetry and  $Z(3)$  interfaces etc. has been discussed in detail in the literature [7, 8]. It has been argued that the  $Z(3)$  symmetry becomes meaningless in the presence of quarks [7]. Other view-point as advocated in many papers, asserts that one can take the effect of quarks in terms of explicit breaking of  $Z(3)$  symmetry [8–10], and we will follow this approach. In this context we mention the recent work of Deka et al. [11] which has provided a support for the existence of these metastable vacua from Lattice. Although the temperatures are high (close to 1 GeV) at which the indications of metastable vacuum are seen in ref.[11], the important point is that these metastable  $Z(3)$  vacua seem to exist at some temperature. Since the presence of quarks lifts the degeneracy of different  $Z(3)$  vacua [8–10], the  $Z(3)$  interfaces become unstable and move away from the region with the unique true vacuum. Thus, with quark effects taken in terms of explicit symmetry breaking, the interfaces survive as non-trivial topological structures, though they do not remain solutions of time independent equations of motion. In our earlier investigations of these  $Z(3)$  walls and the QGP string we had neglected the effects of such an explicit symmetry breaking arising from quark effects [1–3] and had investigated the properties and physical consequences of these objects  $Z(3)$  in the

\*Electronic address: guptausg@gmail.com

†Electronic address: ranjita@iopb.res.in

‡Electronic address: ajit@iopb.res.in

§Electronic address: vivek`krt@hotmail.com

context of early universe as well as in RHICE. In the present work, we will incorporate effects of explicit symmetry breaking from quarks in the study of these objects.

Our numerical simulations in this work aim to investigate how the formation of  $Z(3)$  walls and string network during the initial confinement-deconfinement (C-D) transition in RHICE, and their subsequent evolution, gets affected by such explicit breaking of  $Z(3)$  symmetry. As in our earlier works, we model the pre-equilibrium stage of phase transition in our simulation as a quasi-equilibrium stage with an effective temperature which first rises (with rapid particle production) to a maximum temperature  $T_0 > T_c$ , where  $T_c$  is the critical transition temperature, and then decreases due to continued expansion of plasma.

In order to study the confinement-deconfinement (C-D) phase transition in earlier works for the pure gauge case, we have been using the mean field effective potential of a polynomial form written in terms of the Polyakov loop expectation value  $l(x)$  as proposed by Pisarski [9, 10]. A linear term in  $l(x)$  added to this effective potential in the mean field framework [12–15] accounts for the explicit breaking of  $Z(3)$  symmetry by the dynamical quarks whose presence act like a background magnetic field [16]. In our analysis in ref. [1, 3] we had discussed the effects of the explicit symmetry breaking term in view of the estimates of such a term from ref. [17]. We had found that the two degenerate vacua ( $l = e^{i2\pi/3}$ , and  $l = e^{i4\pi/3}$ ), which get lifted with respect to the true vacuum (with  $l = 1$ ) on account of explicit breaking of  $Z(3)$  symmetry in the QGP phase, have higher free energy than even the hadronic phase (with  $l = 0$ ) at temperatures of order 200 MeV. This does not seem reasonable because one would expect that any of the  $Z(3)$  vacua which become meta-stable due to explicit symmetry breaking should still have lower free energy than the hadronic phase for values of temperature  $T > T_c$  enforcing that the system lies in the deconfining regime for such temperatures. In any case, the estimates of [17] refer to high temperature regime and may not be applicable to temperatures near  $T_c$ . We thus use following considerations to constrain the magnitude of the strength of the explicit symmetry breaking term. One approach can be to limit it such that the metastable vacuum remains lower than the confining vacuum for temperatures above  $T_c$ . We, however, limit explicit symmetry breaking to further lower values by requiring that the first order nature of the transition should remain at least in some range of temperatures above  $T_c$ .

We are using this first order transition model in the present work to discuss the dynamical details of quark-hadron transition, even though the lattice results show that quark-hadron transition is most likely a cross-over at zero chemical potential. The quark-hadron phase transition in the context of relativistic heavy-ion collision experiments is expected to be of first order for not too small values of the chemical potential which may be relevant for our study. Further, we are primarily interested in determining the time dependence of  $Z(3)$  interfaces and string network structures, which result due to explicit breaking of  $Z(3)$  symmetry during the phase transition. The formation of these objects is independent of the nature of phase transition as it results entirely due to finite correlation length in a fast evolving system, as shown by Kibble [18]. The Kibble mechanism was first proposed for the formation of topological defects in the context of the early universe [18], but is now utilized extensively for discussing topological defects production in a wide variety of systems from condensed matter physics to cosmology [19]. Essential ingredient of the Kibble mechanism is the existence of uncorrelated domains of the order parameter which result after every phase transition occurring in finite time due to finite correlation length. A first order transition allows easy implementation of the resulting domain structure especially when the transition proceeds via bubble nucleation. Keeping this view in mind, we use the potential for Polyakov loop augmented with the addition of a linear term as in [9, 10] to model the phase transition. Further we will be confining ourselves to the temperature/time ranges and such values of the coefficient of linear term in the effective potential that the first order quark-hadron transition proceeds via bubble nucleation.

The  $Z(3)$  interfaces and strings will develop dynamics in the presence of explicit symmetry breaking and the interfaces will start moving away from the direction where true vacuum exists. The strings will also not have three interfaces forming symmetrically around it, and hence will start moving in some direction. Such motions may cause important differences on the long time behavior. Due to the quark effects, we will get different nucleation probabilities/rates for the bubbles of meta-stable  $Z(3)$  vacua and the true vacuum bubbles of the QGP phase. Meta-stable bubbles, being larger in size, may cover a larger fraction of the physical space and hence may lead to non-trivial consequences. The effects of quarks will be significant if a closed spherical wall (with true vacuum inside) starts expanding instead of collapsing. This effect may play an important role in the early universe case because an expanding closed domain wall has to be large enough such that the surface energy contribution does not dominate over the volume energy. In the case of RHICE, the asymmetrical  $Z(3)$  walls and associated strings will eventually melt away when the temperature drops below the deconfinement-confinement phase transition temperature  $T_c$ . However they will be leaving their signatures in the form of extended regions of energy density fluctuations (as well as  $P_T$  enhancement of heavy-flavor hadrons [20]). We will be estimating these energy density fluctuations which will lead to multiplicity fluctuations. As in our earlier work [1], here also our main focus will be in looking for the signals of extended regions of large energy densities in space-time reconstruction of hadron density. We mention here that a simulation of spinodal decomposition in Polyakov loop model has been carried out in ref. [21], where fluctuations in the Polyakov loop are investigated in detail. Our work, here and in ref.[1] is focused on the formation of extended structures  $Z(3)$  walls,

strings, and extended regions of energy density etc., and in the present work, how these are affected by effects of quarks.

The paper is organized in the following manner. In section II, we briefly recall the Polyakov loop model of confinement-deconfinement phase transition and describe the effective potential proposed by Pisarski [9]. Here we discuss the effects of quarks in terms of a linear term in the Polyakov loop in the effective potential, which leads to explicit breaking of the  $Z(3)$  symmetry. We discuss different estimates for the strength of this linear term in the context of situations such that the transition is of first order. In section III, we discuss the effect of this term on the structure of  $Z(3)$  walls and strings, and on the structure of bubbles through which the phase transition is completed. Here we describe our approach to extend the conventional technique of false vacuum decay to this case where different  $Z(3)$  bubbles have different profiles. What is of crucial importance to our discussion of the formation of these objects is the nucleation rates of the bubbles of different  $Z(3)$  vacua. Since these vacua are no more degenerate, the corresponding bubbles will in general have different nucleation rates. Section IV discusses nucleation rates for these different bubbles. One may expect that the metastable  $Z(3)$  vacua should be suppressed as the corresponding bubbles have larger actions. We discuss the very interesting possibility that despite having larger action the metastable vacua may have similar (or even larger) nucleation rates as compared to the true vacuum. This can happen when the pre-exponential factor dominates over the exponential suppression term in the nucleation rate. This possibility is intriguing as the metastable vacua, being larger in size, may cover a larger fraction of the physical space and hence may dominate the dynamics of phase transition.

Section V presents the numerical technique of simulating the phase transition via random nucleation of bubbles, which now have different sizes depending on the corresponding  $Z(3)$  vacuum inside the bubble. Resulting domain walls may show non-trivial behavior compared to the case without the quark effects as a closed domain wall, enclosing the true vacuum, may expand instead of contracting. Rough estimates, with our parameter choices, show that this is expected when domain wall size exceeds about 50 fm. The discussion of such a large physical region is more relevant in the context of the early universe and we plan to study this in a future work. Here we will consider the case relevant to RHICE with lattice sizes of about  $(15 \text{ fm})^2$  and study the effects of domain wall and string formation with temperature evolution as expected in a longitudinally expanding plasma. These results are presented in Sec.VI. We also calculate the energy density fluctuations associated with  $Z(3)$  wall network and strings, as in our earlier work [1], and discuss important differences for the present case with quark effects. In section VII we discuss possible experimental signatures resulting from the presence of  $Z(3)$  wall network and associate strings especially including the effects of explicit symmetry breaking. Section VIII presents conclusions.

## II. THE POLYAKOV LOOP MODEL WITH QUARK EFFECTS

We first briefly recall the Polyakov loop model for the confinement - deconfinement phase transition. For the case of pure  $SU(N)$  gauge theory, the expectation value of Polyakov loop  $l(x)$  is the order parameter for confinement - deconfinement phase transition.

$$l(\vec{x}) = \frac{1}{N} \text{Tr}(\mathcal{P} \exp(i g \int_0^\beta A_0(\vec{x}, \tau) d\tau)) \quad (1)$$

Where  $A_0(\vec{x}, \tau)$  is the time component of the vector potential  $A_\mu(\vec{x}, \tau) = A_\mu^a(\vec{x}, \tau) T^a$ ,  $T^a$  are the generators of  $SU(N)$  in the fundamental representation,  $\mathcal{P}$  denotes path ordering in the Euclidean time  $\tau$ ,  $g$  is the gauge coupling, and  $\beta = 1/T$  with  $T$  being the temperature.  $N$  ( $= 3$  for QCD) is the number of colors. The complex scalar field  $l(\vec{x})$  transform under the global  $Z(N)$  (center) symmetry transformation as

$$l(\vec{x}) \rightarrow \exp(2\pi i n/N) l(\vec{x}), \quad n = 0, 1, \dots, (N-1) \quad (2)$$

The expectation value of  $l(x)$  is related to  $e^{-\beta F}$  where  $F$  is the free energy of an infinitely heavy test quark. For temperatures below  $T_c$ , in the confined phase, the expectation value of Polyakov loop is zero corresponding to the infinite free energy of an isolated test quark. (Hereafter, we will use the same notation  $l(x)$  to denote the expectation value of the Polyakov loop.) Hence the  $Z(N)$  symmetry is restored below  $T_c$ .  $Z(N)$  symmetry is broken spontaneously above  $T_c$  where  $l(x)$  is non-zero corresponding to the finite free energy of the test quark. Effective theory of the Polyakov loop has been proposed by several authors with various parameters fitted to reproduce lattice results for pure QCD [9, 10, 22]. We use the Polyakov loop effective theory proposed by Pisarski [9, 10]. The effective Lagrangian density can be written as

$$L = \frac{N}{g^2} |\partial_\mu l|^2 T^2 - V(l) \quad (3)$$

Where the effective potential  $V(l)$  for the Polyakov loop, in case of pure gauge theory is given as

$$V(l) = \left( -\frac{b_2}{2} |l|^2 - \frac{b_3}{6} (l^3 + (l^*)^3) + \frac{1}{4} (|l|^2)^2 \right) b_4 T^4 \quad (4)$$

At low temperature where  $l = 0$ , the potential has only one minimum. As temperature becomes higher than  $T_c$  the Polyakov loop develops a non vanishing vacuum expectation value  $l_0$ , and the  $\cos 3\theta$  term, coming from the  $l^3 + l^{*3}$  term above leads to  $Z(3)$  generate vacua. Now in the deconfined phase, for a small range of temperature above  $T_c$ , the  $l = 0$  extremum becomes the local minimum (false vacuum) and a potential barrier exist between the local minimum and global minimum (true vacuum) of the potential.

To include the effects of dynamical quarks, we will follow the approach where the explicit breaking of the  $Z(3)$  symmetry is represented in the effective potential by inclusion of a linear term in  $l$  [8–10, 12]. The potential of Eq.(4) with the linear term becomes,

$$V(l) = \left( -\frac{b_1}{2} (l + l^*) - \frac{b_2}{2} |l|^2 - \frac{b_3}{6} (l^3 + l^{*3}) + \frac{1}{4} (|l|^2)^2 \right) b_4 T^4 \quad (5)$$

Here coefficient  $b_1$  measures the strength of explicit symmetry breaking. The coefficients  $b_1$ ,  $b_2$ ,  $b_3$  and  $b_4$  are dimensionless quantities. With  $b_1 = 0$ , other parameters  $b_2$ ,  $b_3$  and  $b_4$  are fitted in ref.[9, 10, 23] such that that the effective potential reproduces the thermodynamics of pure  $SU(3)$  gauge theory on lattice [12, 23, 24]. The coefficient  $b_2$  is temperature dependent and given by

$$b_2(r) = \left( 1 - \frac{1.11}{r} \right) \left( 1 + \frac{0.265}{r} \right)^2 \left( 1 + \frac{0.3}{r} \right)^3 - 0.487; \quad r = \frac{T}{T_c}; \quad T_c = 182 \text{ MeV}$$

We use the value of temperature independent coefficients  $b_3 = 2.0$  and  $b_4 = 0.6061 \times \frac{47.5}{16}$ . We choose the same value of  $b_2$  for real QCD (with three massless quarks flavors).  $b_4$  is rescaled by factor  $\frac{47.5}{16}$  to incorporate extra degrees of freedom of QCD relative to pure  $SU(3)$  gauge theory [23]. As temperature  $T \rightarrow \infty$  the Polyakov loop expectation value approaches the value  $x \sim b_3/2 + \frac{1}{2} \sqrt{b_3^2 + 4b_2(T = \infty)}$ . To have the normalization  $\langle l(x) \rangle \rightarrow 1$  at  $T \rightarrow \infty$ , the coefficients and field in the effective potential  $V(l)$  in Eq.(5) are rescaled as  $b_1(T) \rightarrow b_1(T)/x^3$ ,  $b_2(T) \rightarrow b_2(T)/x^2$ ,  $b_3 \rightarrow b_3/x$  and  $b_4 \rightarrow b_4 x^4$ ,  $l \rightarrow l/x$ .

At temperatures above the critical temperature  $T_c$  the potential  $V(l)$  has three degenerate vacua in pure gauge theory (with  $b_1 = 0$ ). The barrier heights between the local minimum ( $l(x) = 0$ ) and the three global minima ( $l = 1, z, z^2$ , corresponding to  $\theta = 0, 2\pi/3, 4\pi/3$ ) are all same. As the value of  $b_1$  becomes non zero, the degeneracy of  $Z(3)$  vacua gets lifted. Vacua corresponding to  $\theta = 2\pi/3$  ( $l = z$ ) and  $\theta = 4\pi/3$  ( $l = z^2$ ) remain degenerate, with energy which is higher than the  $l = 1$  ( $\theta = 0$ ) vacuum. Thus,  $l = z$  and  $l = z^2$  vacua become metastable and the  $l = 1$  remains the only true vacuum (global minimum). Note that  $l = z$  and  $l = z^2$  are the two metastable vacua in the QGP phase. Along with these, there is a metastable vacuum at  $l = 0$  (for a small range of temperature above  $T_c$ ) which corresponds to the confining phase.

Estimates of explicit  $Z(3)$  symmetry breaking arising from quark effects have been discussed in the literature. In the high temperature limit, the estimate of the difference in the potential energies of the  $l = z$  vacuum, and the  $l = 1$  vacuum,  $\Delta V$ , is given in ref. [17] as,

$$\Delta V \sim \frac{2}{3} \pi^2 T^4 \frac{N_l}{N^3} (N^2 - 2) \quad (6)$$

where  $N_l$  is the number of massless quarks. If we take  $N_l = 2$  then  $\Delta V \simeq 3T^4$ . At  $T = 200$  MeV, the difference between the confining vacuum and the true vacuum from the effective potential in Eq.(5) is about  $150 \text{ MeV/fm}^3$  while  $\Delta V$  from Eq.(6) at  $T = 200$  MeV is about four times larger, equal to  $600 \text{ MeV/fm}^3$ . As  $T$  approaches  $T_c$ , this difference will become larger as the metastable vacuum and the stable vacuum become degenerate at  $T_c$ , while  $\Delta V$  remains non-zero. It does not seem reasonable that at temperatures of order 200 MeV (with  $T_c = 182$  MeV for Eq.(5)) a QGP phase (with quarks) has higher free energy than the hadronic phase. In any case, the estimates of

Eq.(6) were made in high temperature limit and the extrapolation of these to  $T$  near  $T_c$  may be invalid. We, thus, use different physical considerations to estimate the strength of the explicit symmetry breaking term, i.e. the value of parameter  $b_1$  in Eq.(5), as follows.

Note that as  $b_1$  is increased from zero, the potential tilts such that the barrier between the metastable confining phase and the true vacuum in the  $\theta = 0$  direction decreases, resulting in the weakening of the first order phase transition. Finally, this barrier disappears for  $b_1 \geq 0.11$  (at  $T = T_c = 182$  MeV). For  $b_1 \geq 0.11$  there is no range of temperature where the phase transition is first order. As we mentioned, our approach is to study the phase transition dynamics via bubble nucleation. We thus choose a small value of  $b_1 = 0.005$  such that the confinement - deconfinement phase transition is (weakly) first order phase transition for a reasonable range of temperature. The plot of the potential in  $\theta = 0$  direction for  $b_1 = 0.005$  is shown in Fig.1 for  $T = 200$  MeV. Note that with  $b_1 > 0$  the confining vacuum at  $l = 0$  shifts towards positive real value of  $l$ . With this value of  $b_1$ , the barrier between the confining metastable vacuum and the true vacuum exists upto temperature  $\simeq 225$  MeV which allows for a reasonable range of temperatures to discuss the bubble profiles and their nucleation probabilities. If we choose larger values of  $b_1$ , the range of temperature allowing first order transition becomes very narrow and formation and nucleation of bubbles require fine tuning of time scale.

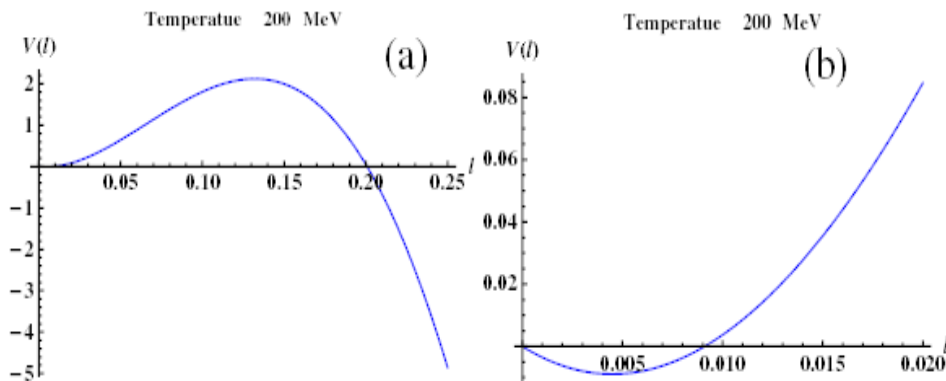


FIG. 1:

- (a) Plot of  $V(l)$  (in  $\text{MeV}/\text{fm}^3$ ) in  $\theta = 0$  direction for  $T = 200 \text{ MeV}$  with  $b_1 = 0.005$ . (b) shows the plot near the origin, showing that the confining vacuum has shifted slightly from  $l = 0$  towards  $\theta = 0$  direction.

This, apparently ad hoc, procedure of fixing value of  $b_1$  can be given a physical basis in the following way. Changing the value of coefficient  $b_1$  changes the nature of phase transition from very strong first order to a very weak one. One can attempt to interpret it in the context of QCD phase diagram, drawn in the plane of chemical potential ( $\mu$ ) and temperature ( $T$ ). The QCD phase transition is of strong first order for large  $\mu$ , it becomes a weak first order transition with decreasing  $\mu$ , reaches to critical end point where the transition is of second order and then becomes crossover at lower  $\mu$  values. If we assume that the effective potential in Eq.(5) (at least in form) can describe these situations of varying chemical potential, then it looks natural to assume that changing the value of  $\mu$  is interpreted in terms of changing the value of  $b_1$  parameter in Eq.(5). Thus increasing  $\mu$  corresponds to lowering the value of  $b_1$  making the phase transition of stronger first order.

Note that the potential barrier between the confining vacuum and the true vacuum is maximum when  $b_1$  is zero and the first order phase transition is strongest. This should correspond to the situation of largest  $\mu$  according to the above argument, presumably corresponding to the transition at very low temperatures in the QCD phase diagram. However, with  $b_1 = 0$  there is no explicit symmetry breaking. This will not be consistent with the expectation of explicit symmetry breaking arising from quark effects. Though one cannot exclude the possibility that the effects of dynamical quarks and that of net baryon number density may have opposite effects on the value of  $b_1$ , so that a strong first order transition at large  $\mu$  can be consistently interpreted in terms of  $b_1 = 0$ . However, it is simpler to assume that even for the largest value of  $\mu$  (where the first order curve intersects the  $\mu$  axis in the QCD phase diagram),  $b_1$  never becomes zero so that explicit symmetry breaking remains present as expected.

Of course, it is clear that the parameter values used in Eq.(5), which were fitted using lattice results for  $\mu = 0$  case, are no longer applicable, if non-zero values of  $b_1$  are interpreted in terms of non-zero  $\mu$ . We will then need to assume that the required changes in the parameters of Eq.(5) for non-zero  $\mu$  are not large. At the very least we can say that, even if  $b_1$  values we use here cannot be justified, they help us capture some qualitative aspects of changes in the formation and evolution of  $Z(3)$  walls and QGP strings when quark effects are incorporated.

### III. DOMAIN WALLS, STRINGS AND BUBBLES WITH EXPLICIT SYMMETRY BREAKING

The explicit symmetry breaking arising from quark effects will have important effects on the structure of topological objects;  $Z(3)$  walls and the QGP strings. It will obviously also affect the nucleation of bubbles of different  $Z(3)$  phases. First we qualitatively discuss its effects on  $Z(3)$  walls and the QGP strings. For non-degenerate vacua, even planar  $Z(3)$  interfaces do not remain static, and move away from the region with the unique true vacuum. Thus, while for the degenerate vacua case every closed domain wall collapses, for the non-degenerate case this is not true any more. A closed wall enclosing the true vacuum may expand if it is large enough so that the surface energy contribution does not dominate. Similarly it is no more possible to have time independent solution for the QGP string. Without explicit symmetry breaking a QGP string forming at the intersection of three symmetrically placed  $Z(3)$  walls will be stationary. However, with  $b_1 \neq 0$  this is not possible for any configuration of domain walls. In fact this type of situation has been discussed in the context of early universe for certain types of anionic string models [25].

Apart from the structure of these objects, one also expects important changes in the basic mechanism of formation of these objects during phase transition. Without explicit symmetry breaking, these objects will form via the Kibble mechanism, as discussed in detail in [1]. In the presence of explicit symmetry breaking new effects may arise as discussed in [26] where many string-antistring pairs with small separations (which means small loops of strings or small closed domain walls in the present context) can form at the coalescence region of two bubbles. This mode of production of topological objects arises from the fluctuations of the order parameter and is entirely different from the basic physics of the Kibble mechanism. As we are using very small value of explicit symmetry breaking, we do not expect this new mechanism to play an important role here. However, for larger values of  $b_1$ , this production mechanism may play an important role in determining the  $Z(3)$  wall and string network resulting from a first order QCD phase transition.

General picture of the formation of these objects during first order QCD transition via bubble nucleation was described in detail in ref. [1] for the case without explicit symmetry breaking and we briefly summarize it below. Subsequently we will discuss the effects of explicit symmetry breaking on the bubble profiles, their nucleation rates, and on general dynamics of the phase transition.

We calculate the bubble profile of QGP phase using Coleman's technique of bounce solution [27] for true vacuum ( $l = 1$ ) and for metastable vacua ( $l = z, z^2$ ). We seed these bubbles in the false (hadronic) background randomly with their nucleation rates calculated at an appropriate value of temperature  $T > T_c$  (such that the nucleation rate is appreciable). The value of the phase of the complex order parameter  $l$  is constant inside a given bubble (to minimize the free energy), while it changes from one bubble to another randomly (corresponding to the choices of three vacua). The variation of the orientation of the order parameter from one bubble to another provides the essential ingredient of the Kibble mechanism leading to a domain structure and formation of topological objects at the intersection of domains. We evolve this initial field configuration with the equations of motion using leap frog algorithm. Bubbles grow with time and coalesce with each other. The bubbles with same vacuum merge together to form a bigger region of same vacuum while the bubbles with different vacua remain separated by a wall/interface of high energy density after coalescence. These are the  $Z(3)$  domain walls. These domain walls are solutions of field equations of motion, interpolating between different  $Z(3)$  vacua, and survive till very long time as QGP evolves. Eventually, either walls collapse/merge away, or they melt as the temperature of expanding QGP falls below  $T_c$  and  $Z(3)$  symmetry is restored.

Spontaneous breaking of  $Z(3)$  symmetry in the QGP phase leads to three different topological domain walls separating the three different  $Z(3)$  vacua. The intersection point of the three domain walls leads to a topological string (the QGP string) which was discussed in detail in ref. [2]. This string arises as the order parameter  $l$  completes a closed loop around  $l = 0$  in the complex  $l$  space when one encircles the intersection point of the three domain walls in the physical space [2]. Thus, these are topological strings which exist in the QGP phase and have confining core (with  $l = 0$ ). As bubbles of different  $Z(3)$  vacua coalesce with each other, a network of  $Z(3)$  walls forms and at the intersection of  $Z(3)$  walls, QGP strings form. A detailed investigation of this for the case without explicit symmetry breaking (i.e.  $b_1 = 0$ ), using 2+1 dimensional simulation representing the central rapidity region, was carried out in ref. [1].

The above picture of the dynamics of bubble nucleation, coalescence, and formation and evolution of  $Z(3)$  walls and QGP strings will be affected by the presence of explicit symmetry breaking in important ways. With  $b_1 \neq 0$ , the three  $Z(3)$  vacua are no longer degenerate. The two vacua ( $l = z, z^2$ ) corresponding to  $\theta = 2\pi/3, 4\pi/3$  get lifted and become metastable. Only the third one with real expectation value of  $l$  remains stable. The energy difference between the confining vacuum (near  $l = 0$ , note that due to  $b_1 \neq 0$ , the confining vacuum shifts slightly) and the two metastable  $Z(3)$  vacua (with  $l = z, z^2$ ) is smaller than the energy difference between the confining vacuum and the true vacuum. This leads to larger bubble size for metastable vacuum than the bubble of true vacuum, with larger value of associated action (free energy). The energy difference between the confining vacuum and true or metastable vacuum increases with increase in temperature so the bubble sizes decreases with increase in temperature.

In the non-degenerate case with non vanishing explicit symmetry breaking the false vacuum of potential gets

shifted towards real axis by an small amount  $\epsilon$ . This shift is minimum for temperature closer to  $T_c$  and increases as we increase the temperature. Further, the local maximum of the potential barrier and the metastable vacua are not in same direction but there is a small angular shift between them. These aspects make it difficult to apply the Coleman's technique of bounce solution of a scalar field for the present case as we will discuss below. First we review the basic features of the first order transition via bubble nucleation.

A first order phase transition proceeds by the nucleation of a true vacuum bubble in the background of false vacuum. A true vacuum bubble produced, will grow or collapse depending on the free energy change of the system. The change in the free energy of the system because of the creation of a true vacuum bubble of radius  $R$  is

$$F(R) = F_s + F_v = 4\pi R^2 \sigma - \frac{4\pi}{3} R^3 \eta \quad (7)$$

Here  $F_v$  is the volume energy and  $F_s$  is the surface energy of the bubble. For a strong first order phase transition, one can analytically determine the potential energy difference  $\eta$  between the confining vacuum and relevant  $Z(3)$  vacuum and the surface tension  $\sigma$  from bounce solution (at least for a scalar field). Minimization of this free energy determines the critical radius  $R_c = \frac{2\sigma}{\eta}$ . The volume energy of the bubbles with radius  $R > R_c$  dominates over its surface energy and the bubbles expand to transform the false vacuum to true vacuum. The smaller bubbles ( $R < R_c$ ) for which surface energy dominates over the volume energy, shrink and disappear. For strong first order transition, calculation of  $\eta$  and  $\sigma$  separately can be done as one is dealing with the thin wall bubbles where the bubble size is much larger than the thickness of the bubble wall, so that there is clear separation between the bubble core and the bubble wall. For the parameter values, and the temperature range of our interest, we will be dealing with thick wall bubbles where bubble size is of the same order as the bubble wall. For this purpose, the expression in Eq.(7) is not of use, and one has to calculate the bubble profile numerically using Coleman's technique of bounce solution and determine its action to calculate nucleation probabilities.

The theory of semiclassical decay of false vacuum at zero temperature is given in ref [27] and its extension to finite temperature was given in ref [28]. The Coleman's technique is applicable for real scalar field. To calculate bubble profile for complex scalar field  $l$  (with  $b_1 = 0$ ), in ref. [1], the phase angle  $\theta$  was taken to be constant by fixing it in the direction of the relevant  $Z(3)$  vacuum, i.e.  $\theta = 0, 2\pi/3, \text{ or } 4\pi/3$ . This reduced the problem again to a real scalar field calculation and Coleman's technique could be directly applied. (However, there are important issues for the case of complex scalar field regarding the calculation of nucleation rates which require calculation of determinant of fluctuations around the bounce solution. A brief discussion of these issues is provided in ref. [1].

We calculate the bubble profile in  $3 + 1$  dimension. However, we evolve it only by the  $2 + 1$  dimensional field equations. This is because of rapid longitudinal expansion which simply stretches the bubbles in the longitudinal direction, while its transverse evolution proceeds according to field equations. We neglect the transverse expansion of system which is certainly a good approximation during early stages of bubble nucleation (during initial transition from confining phase to the QGP phase with time scales of order 1 fm). At finite temperature, the  $3+1$  - dimensional theory will reduce to an effectively 3 Euclidean dimensional theory if the temperature is sufficiently high, which we will take to be the case [1]. For this 3 dimensional Euclidean theory, the bubble profile is the solution of the following equation

$$\frac{d^2 l}{dr^2} + \frac{2}{r} \frac{dl}{dr} = \frac{g^2}{2NT^2} \frac{\partial V}{\partial l} \quad (8)$$

where  $r = r_E = \sqrt{\vec{x}^2 + t_E^2}$ , subscript E denotes coordinates in the 3 dimensional Euclidean space. We use fourth order Runge-Kutta method to solve Eq.(8). For  $b_1 = 0$ , the relevant boundary conditions on  $l$  to calculate the bubble profile are  $l = 0$  as  $r \rightarrow \infty$  and  $\frac{dl}{dr} = 0$  at  $r = 0$ . However, with  $b_1 > 0$  this is no longer applicable. This is because with  $b_1 \neq 0$  the confining vacuum is shifted from  $l = 0$  along  $\theta = 0$  direction by an amount  $\epsilon$ . We calculate the bubble profile at  $T = 200$  MeV and at this temperature  $\epsilon = 0.0045$  (see, Fig.1b). We thus re-write the effective potential in Eq.(5) in terms of a shifted field  $l' = l - \epsilon$ . In terms of  $l'$  the confining vacuum again occurs at  $l' = 0$  and the standard boundary conditions as discussed above can be applied for solving Eq.(8) for the bounce solution. Hereafter all discussion will be in terms of this shifted field  $l'$  which, for simplicity we will denote as  $l$  only.

Another complication occurs in calculating the bubble profile for the metastable  $Z(3)$  vacua. The earlier technique for  $b_1 = 0$  case of simply fixing  $\theta = 2\pi/3$  or  $\theta = 4\pi/3$  for the two respective vacua, thereby reducing the problem to a real scalar field case, cannot be applied here directly. This is because with  $b_1 \neq 0$ , the maximum of the respective potential barrier and direction of the corresponding metastable vacuum are not in the same direction (due to the tilt of the potential resulting from  $b_1 \neq 0$ ). However, the difference between the two directions, i.e. between the  $l = z$  vacuum and the direction of the top of the corresponding barrier, is very small, of order  $\theta = 0.9^\circ$ . Same is true for  $l = z^2$  vacuum. We then fix  $\theta$  along  $l = z$  and  $l = z^2$  vacua respectively to get the approximately valid bubble profile

using Eq.(8). (Both these directions differ slightly from  $\theta = 2\pi/3$  and  $\theta = 4\pi/3$  now. Note again all this is using the shifted field which we are again denoting as  $l$ .) Recall, that we are calculating 3+1 dimensional critical bubble and evolving it by 2+1 dimensional equations with the bubble becoming supercritical for 2+1 dim. equations [1]. Further we are studying the situation of rapidly changing temperature. Thus exact profile of the critical bubble at the nucleation time if not of much relevance.

As we had mentioned above, we choose the value of  $b_1$  such that the barrier between the confining vacuum and various  $Z(3)$  vacua remains non-zero up to some range of temperature so that bubble formation can be carried out. We choose  $b_1 = 0.005$  with which the barrier between the confining vacuum and true vacuum exist upto temperature  $\simeq 225$  MeV. The first order phase transition via bubble nucleation is possible only upto this temperature.

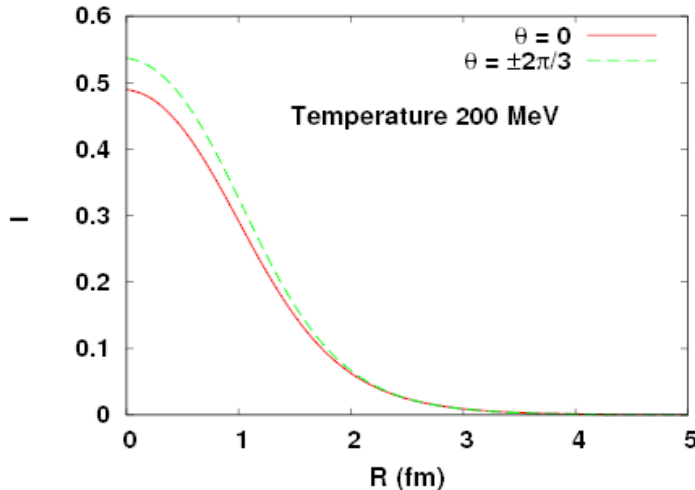


FIG. 2:  
Critical bubble profiles for the different  $Z(3)$  vacua for  $b_1 = 0.005$ .

#### IV. NUCLEATION RATES FOR DIFFERENT BUBBLES

For the finite temperature case, the tunneling probability per unit volume per unit time in the high temperature approximation is given by [28] (in natural units)

$$\Gamma = A e^{-S_3(l)/T} \quad (9)$$

where  $S_3(l)$  is the 3-dimensional Euclidean action for the Polyakov loop field configuration that satisfies the classical Euclidean equations of motion. The dominant contribution to the exponential term in  $\Gamma$  comes from the bounce solution which is the least action  $O(3)$  symmetric solution of Eq.(8). For a theory with one real scalar field in three Euclidean dimensions the pre-exponential factor arising in the nucleation rate of critical bubbles has been estimated, see ref. [28]. The pre-exponential factor obtained from [28] for our case becomes

$$A = T^4 \left( \frac{S_3(l)}{2\pi T} \right)^{3/2} \quad (10)$$

As emphasized in [1], the results of [28] were for a single real scalar field and one of the crucial ingredients used in [28] for calculating the pre-exponential factor was the fact that for a bounce solution the only light modes contributing to the determinant of fluctuations were the deformations of the bubble perimeter. Even though we are discussing the case of a complex scalar field  $l(x)$ , this assumption may still hold as we are calculating the tunneling from the false vacuum to one of the  $Z(3)$  vacua. This assumption may need to be revised when light modes e.g. Goldstone bosons are present which then also have to be accounted for in the calculation of the determinant.



A somewhat different approach for the pre-exponential factor in Eq.(9) is obtained from the nucleation rate of bubbles per unit volume for a liquid-gas phase transition as given in ref. [29, 30]. In ref.[1] we had considered these estimates for the nucleation rate as well as those obtained from Eq.(10). It was found that for the parameter values in Eq.(5) and for the temperature/time scales relevant for RHICE, the nucleation rates obtained using the liquid-gas transition approach of ref.[29, 30] were completely negligible such that even nucleation of one bubble of QGP phase was not likely at RHICE. As one needs several bubbles to discuss the formation of Z(3) walls and strings, these estimates clearly cannot be used here. As in ref.[1] we will follow the approach based on Eq.(10) for our case which gave reasonable nucleation rates leading to the possibility of formation of several bubbles for the case of RHICE. We may mention here that for nucleation of bubbles of the Polyakov loop  $l$  it may anyway be better to use a field theory approach as in ref.[28] rather than the approach of ref. [29, 30] which is more suitable for the description of phase transition in terms of plasma degrees of freedom. Though, the parameters of Eq.(5) have been fitted with lattice QCD, it is still not very clear whether the bubbles should be viewed in terms of an order parameter field representing some background condensate (as the Polyakov loop  $l$ ), or just different phases of an interacting plasma.

We thus proceed with the calculation of nucleation rates of the bubbles using Eqs.(9),(10). Fig.2 shows the profiles of the bubbles for  $l = 1$  and  $l = z$  vacua at  $T = 200$  MeV ( $l = z^2$  bubbles has the same profile as the  $l = z$  bubble). We note that  $l = z$  bubble is somewhat larger as expected. Using such bubble profiles we calculate the respective values of the action  $S_3$  and estimate the nucleation rates for metastable and true vacuum at different temperatures. To calculate number of bubbles for a typical nucleus nucleus collision, we consider a circle of 8 fm radius in transverse plane with 1 fm thickness in the longitudinal direction. The bubble nucleation for 1 fm time obtained from the nucleation rate given in Eqs.(9),(10) leads to about 3 - 5 bubbles in this region. (The approach followed in ref. [30] gives the nucleation rate of about  $10^{-4}$  fm $^{-4}$  in the relevant temperature range, leading to negligible nucleation of bubbles).

One may expect that nucleation rate of the two metastable Z(3) vacua will be smaller than that of the true Z(3) vacuum due to larger action  $S_3$  of the metastable vacuum leading to exponential suppression. However, here we see an interesting interplay between the exponential factor  $e^{-S_3(T)/T}$  (Eq.(9)) and the prefactor  $A$  as given in Eq.(10). If  $S_3(T)$  is much larger than  $T$  then the nucleation rate is dominated by the exponential factor confirming the above expectation. Thus, the nucleation rate of metastable vacuum bubble is much smaller than the true vacuum bubble when temperature is closer to  $T_c$ . The nucleation rate of true vacuum bubble and metastable vacuum bubble at temperature near  $T_c$  (at  $T = 185$  MeV) is of the order of  $\sim 1.3 \times 10^{-5}$  fm $^{-4}$  and  $\sim 3.4 \times 10^{-7}$  fm $^{-4}$  respectively. As we increase the temperature from  $T_c = 182$  MeV, the nucleation rate of metastable vacuum bubble increases and becomes almost equal to that of true vacuum bubble at  $T \simeq 200$  MeV (both rates being about  $\sim 2.4 \times 10^{-2}$  fm $^{-4}$ ). This happens because at these temperatures  $S_3 \simeq T$  so that the decrease of the exponential term for a larger  $S_3$  (corresponding to the metastable vacuum) is not very significant. However, the pre-exponential factor  $A$  in Eq.(10) increases with  $S_3$  and this increase of the prefactor term starts dominating the exponential factor in the nucleation rate equation for  $T \geq 200$  MeV. For larger temperatures, the nucleation rate for metastable vacuum bubbles become larger than the true vacuum bubbles. The nucleation rates of metastable and true vacuum bubble at temperature 215 MeV are the order of  $\sim 1.5 \times 10^{-2}$  fm $^{-4}$  and  $7.7 \times 10^{-3}$  fm $^{-4}$  respectively. At higher temperatures though the nucleation rate for both bubbles decrease but the metastable bubble nucleation rate remains larger. This result is very interesting as it shows that at suitable temperatures the metastable Z(3) vacua will have larger nucleation rate than the true Z(3) vacuum. Further, these metastable vacuum bubbles are also of larger size than the bubble of true vacuum. Thus one may expect a larger fraction of the QGP region to end up in the metastable Z(3) vacuum regions after the phase transition which may have interesting implications. For example, we will see below that the metastable vacuum bubble walls have much higher concentration of energy density than the true vacuum bubble walls. We will use  $T = 200$  MeV for the bubble nucleation as the nucleation rate are same for both the true vacuum and metastable vacuum bubbles.

## V. NUMERICAL TECHNIQUES

In this work, we carry out a 2 + 1 dimensional field theoretic simulation of the formation and evolution of QGP phase bubbles representing the central rapidity region of QGP in RHICE. Bubbles are nucleated randomly in the confining background. We calculate the bubble profiles in 3 + 1 dimension and use these profiles for the evolution in 2+1 dimensions. As explained above, this represents transverse evolution of these bubbles by field equations and their longitudinal evolution is simply given by the Bjorken longitudinal expansion [31]. We nucleate bubbles at the temperature 200 MeV at which the metastable and true vacuum bubbles have the nucleation rates of the same order  $\simeq 0.024$  fm $^{-4}$  so that the number of metastable and true vacuum bubbles seeded remains almost equal. Initially the the field  $l(\vec{x})$  is zero every where and bubbles of QGP phase are nucleated over the whole lattice with random choice of their location. (Again, recall that we are using the shifted field here with  $b_1 \neq 0$ ). Bubbles are nucleated with the

condition that one bubble should not overlap with the other. We implement this condition by checking that whether the region where bubble is going to be nucleated, lies in the false vacuum or not. If in the region a bubble has seeded already, the next bubbles will be seeded at some other random position with same conditions. (These techniques for the formation and evolution of bubbles in a first order transition are the same as used in ref.[32].)

We take the initial temperature of the system to be zero (representing initial confining system) and it is taken to increase linearly with time up to  $T = 400$  MeV, at (proper) time  $\tau = \tau_0 = 1$  fm. The bubble nucleation is possible only in the range of temperature where the transition is of first order. The barrier in between false vacuum and true vacuum as well as false vacuum and metastable vacua of Eq.(5) exist only for the temperature  $T = 182$  MeV to  $T \simeq 225$  MeV for our chosen value of  $b_1 = 0.005$ . The nucleation of bubbles is possible only during the time when temperature linearly increases from  $T = T_c = 182$  MeV to  $T \simeq 225$  MeV. In order to have a reasonable range of temperatures for bubble nucleation and evolution we nucleate bubbles at  $T = 200$  MeV. Note that bubbles should also be nucleated at higher temperatures, say near  $T = 225$  MeV. These will be smaller in size. Along with such bubbles there will also be subcritical bubble which shrink fast and disappear due to the surface energy domination. Such bubbles should be incorporated to account for fluctuations [32], but we will ignore these here.

In Relativistic Heavy Ion Collision Experiments the QGP bubbles are nucleated in the hadronic phase during the time span when temperature changes from the transition temperature to the maximum temperature  $T_0 = 400$  MeV in the pre-equilibrium stage, hence this should lead to the presence of metastable and true vacuum bubbles of different sizes at a given time. These bubbles expand in hadronic background with time and ultimately the whole system gets converted to the QGP phase. We choose to seed the bubbles at a fix nucleation temperature because the QGP bubbles being nucleated in hadronic background have zero velocity initially and remain almost static during the remaining pre-equilibrium time  $\simeq 0.5$  fm when temperature increases from  $T = T_c = 182$  MeV to  $T = T_0 = 400$  MeV. The growth of bubbles nucleated at different time and the increase in their velocity until the temperature reaches to 400 from the nucleation temperature, are negligible in this short time span. Therefore our choice for simplicity to seed bubbles at fixed temperature is a reasonable approximation. We choose  $T = 200$  MeV as at this temperature the true vacuum and the metastable vacuum bubbles have almost equal nucleation rate and both kind of bubbles are possible with equal probability. This provides us a better opportunity to study the dynamics of metastable vacuum bubbles together with that of true vacuum bubbles and its effect on true vacuum bubbles evolution.

After nucleation, bubbles are evolved by time dependent equation of motion in the Minkowski space [33]

$$\frac{\partial^2 l_j}{\partial \tau^2} + \frac{1}{\tau} \frac{\partial l_j}{\partial \tau} - \frac{\partial^2 l_j}{\partial x^2} - \frac{\partial^2 l_j}{\partial y^2} = -\frac{g^2}{2NT^2} \frac{\partial V(l)}{\partial l_j}; \quad j = 1, 2 \quad (11)$$

with  $\frac{\partial l_j}{\partial \tau} = 0$  at  $\tau = 0$  and  $l = l_1 + il_2$ .

We take a  $2000 \times 2000$  lattice with physical size 16 fm x 16 fm. (as appropriate for, say Au-Au collision at RHICE). We take this lattice as the transverse plane of the QGP formed in a central collision and consider the longitudinal extension of 1 fm in the mid rapidity region. The evolution of metastable and true vacuum bubbles with different  $Z(3)$  vacuum inside gives rise to the domain wall and string networks. The domain walls form when the two bubbles of different  $Z(3)$  vacua coalesce with each other. The intersection of three domain walls forms a string. In our simulation these objects are formed in the transverse plane. Hence, the domain walls appear as curves while the cross section of three dimensional strings appear as vortices.

In the relativistic heavy ion collision, the thermalization time for a Au - Au collision at 200 MeV is expected to be  $\tau \leq 1$  fm time. As mentioned above, we model the system in our simulation such that there is a linear increase in temperature in the pre-equilibrium stage. It starts from  $T = 0$  and reaches to a maximum value of  $T = 400$  within time  $\tau = 0$  to  $\tau = \tau_0 = 1$ . After that it decreases according to Bjorken's scaling due to the continued expansion in longitudinal direction [31]

$$T(\tau) = T(\tau_0) \left( \frac{\tau_0}{\tau} \right)^{1/3} \quad (12)$$

In our numerical simulation we evolve the field using the periodic, fixed, and free boundary conditions for the square lattice. We present our results for the free boundary condition case where the field (waves) crossing the boundary during evolution go out permanently. This condition minimizes effects due to boundary points in the evolution of field (field reflection from boundary points in fixed boundary condition and mirror reflection as in periodic boundary condition). We use additional dissipation in a thin strip of ten points near the boundary to reduce the (minor) boundary effects in the use of free boundary conditions. For representing the situation of heavy ion collision experiments we nucleate bubbles within a circular region of 8 fm radius on the lattice of physical size 16 fm x 16 fm. With  $\Delta x = 0.008$  fm, we use  $\Delta t = \Delta x/\sqrt{2}$  and  $\Delta t = 0.9\Delta x/\sqrt{2}$  to satisfy the Courant stability criteria.

The stability and accuracy of the simulation is checked using the conservation of energy during simulation. The total energy fluctuations remains few percent without any net increase or decrease of total energy in the absence of dissipative  $\dot{l}$  term in Eq.(11) as well as any other dissipation for periodic and fixed boundary condition.

## VI. RESULTS OF THE SIMULATION

General picture of the phase transition remains similar to the case of  $b_1 = 0$  discussed in [1], but there are important differences. We show in Fig. 3 the various stages of the formation and evolution of different Z(3) bubbles and subsequent formation and evolution of Z(3) walls and strings. In order that one can compare with the case discussed in ref.[1] for  $b_1 = 0$  case, we present in Fig.3 the case of 5 bubbles in a 16 fm  $\times$  16 fm region, similar to the case discussed in ref.[1]. Fig.3a shows the initial plot of  $l(x)$  showing nucleation of 5 bubbles at  $\tau = 0.5$  fm. Fig.3b shows the plot of  $l(x)$  at  $\tau = 1.5$  fm showing the expansion of bubbles. Fig.3c shows the plot of the phase of  $l(x)$  at the initial stage and Fig.3d shows the phase plot at  $\tau = 3.2$  fm showing clearly the formation of domain walls and a QGP string near  $(x=8 \text{ fm}, y=9 \text{ fm})$ . The important difference in the dynamics of true vacuum bubbles and the metastable vacuum bubbles can be seen in the surface plots of energy density (in GeV/fm<sup>3</sup>) at  $\tau = 0.75$  fm (Fig.3e) and at  $\tau = 2.6$  fm (Fig.3f). Note that in all the figures we plot energy density in GeV/fm<sup>3</sup> as we are considering the central rapidity region with thickness of about 1 fm. With similar energy densities to begin with, by the time  $\tau = 2.6$  fm, the energy density at the walls of bubbles of true vacuum is much smaller than the energy density of walls for the false vacuum bubbles.

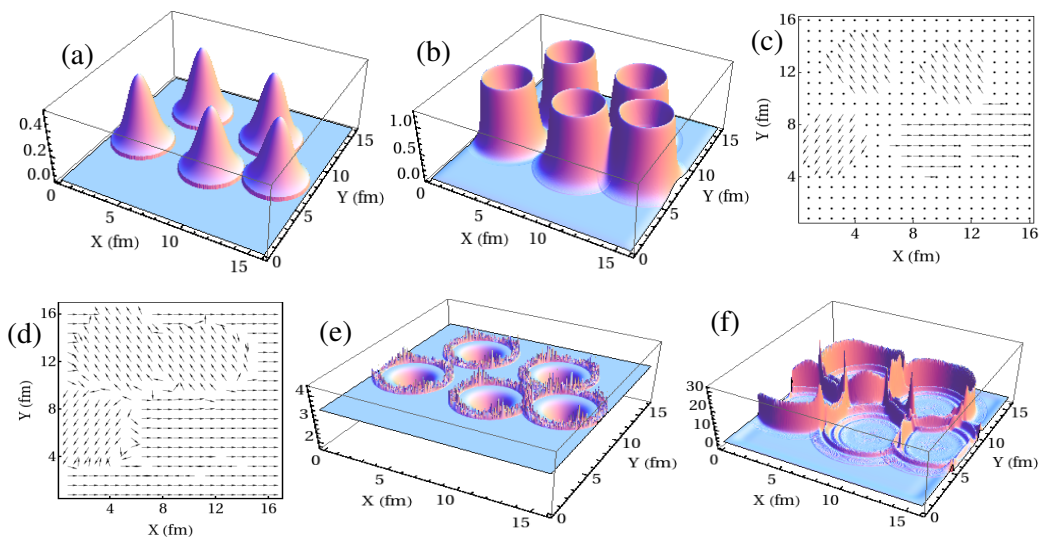


FIG. 3:

(a) and (b) show plots of profiles of  $l$  at  $\tau = 0.5$  fm and 1.5 fm respectively showing expansion of bubbles. (c),(d) show the plots of the phase of  $l$  at  $\tau = 0.5$  and 3.2 fm. (e) and (f) show the surface plots of energy density (in GeV/fm<sup>3</sup>) at  $\tau = 0.75$  and 2.6 fm showing very different energetics of the walls of the true vacuum bubbles and the metastable vacuum bubbles.

### A. variance of energy density

General evolution of bubble coalescence and formation of walls and strings are similar to those shown in ref.[1] for the  $b_1 = 0$  case and we do not show those here. As we are discussing the case of relatively small value of  $b_1$  here we do not expect dramatic effects arising from explicit symmetry breaking (e.g. from the different mechanism of production of topological objects as demonstrated in ref.[26]). However, it is still important to see if there are any qualitative differences between the  $b_1 = 0$  case and  $b_1 \neq 0$  case. We find an interesting difference in the plot of the variance of energy density between the two cases. We calculated the variance of energy density  $\Delta\varepsilon$  at each time stage to study how energy fluctuations change during the evolution. In Fig.4 we show the plot of  $\Delta\varepsilon/\varepsilon$  as a function of proper time. Here  $\varepsilon$  is the average value of energy density at that time stage. The energy density  $\varepsilon$  decreases due to longitudinal expansion, hence we plot this ratio to get an idea of relative importance of energy density fluctuations.

For comparison we reproduce such a plot from ref.[1] for  $b_1 = 0$  case in Fig.4b. We note that fluctuations have an overall tendency to decrease in Fig.4b while there seems no such decrease in Fig.4a for the case with quark effects. Note also the presence of a peak for small times near  $\tau \simeq 3$  fm in  $b_1 > 0$  case. There is no such sharp peak for  $b_1 = 0$  case. Remaining features of the plot can be interpreted as follows. The initial rapid drop in  $\Delta\varepsilon/\varepsilon$  is due to large increase in  $\varepsilon$  during the heating stage upto  $\tau = 1$  fm, followed by a rise due to increased energy density fluctuations during the stage when bubbles coalesce and bubble walls decay, as expected. The peak in the plot near  $\tau = 10$  fm when  $T$  drops below  $T_c$  should correspond to the decay of domain walls and may provide a signal for the formation and subsequent decay of such objects in RHICE.

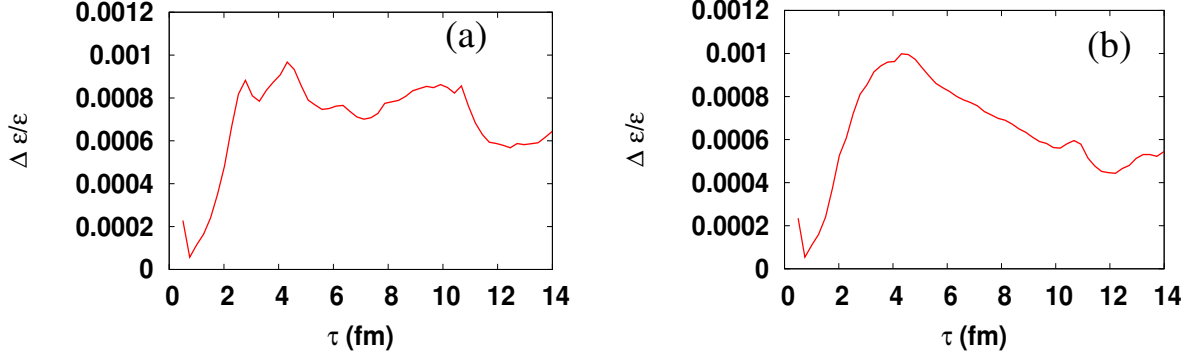


FIG. 4:

(a) and (b) show plots of the ratio of variance of energy density  $\Delta\varepsilon$  and the average energy density  $\varepsilon$  as a function of proper time for  $b_1 = 0.005$  case and  $b_1 = 0$  case respectively.

The small peak at short times for  $b_1 > 0$  case seems to arise from the difference between the collisions of metastable vacuum bubbles and true vacuum bubbles and hence seems of qualitative importance. We have checked for various situations, different number of bubbles etc. and this peak is always present. Fig.5 shows different cases, for number of bubbles ranging from 4 to 10 and we see the presence of this peak in all these cases.

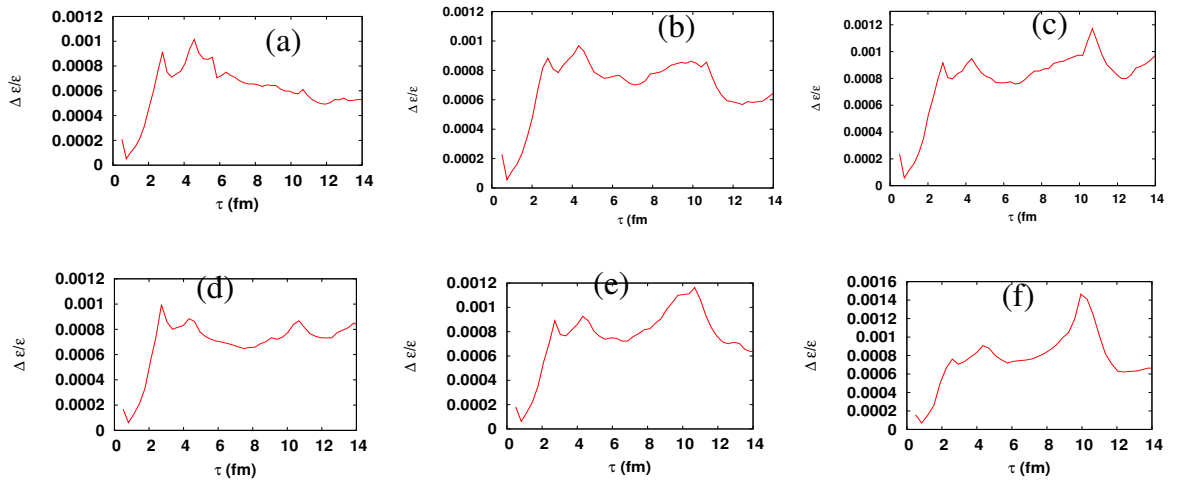


FIG. 5:

Plots of the ratio  $\Delta\varepsilon/\varepsilon$  as a function of proper time for  $b_1 = 0.005$  case for different number of bubbles. (a) - (f) show curves for number of bubbles = 4,5,5(different realization),7,8, and 10, respectively. Note the presence of small peak for short times in all these cases. Also note that there is no overall decrease for large times as was seen in Fig.4b for  $b_1 = 0$  case.

### B. wall velocity

An important difference we note is in the wall velocity. We have estimated wall velocities for the domain walls separating the two degenerate metastable  $Z(3)$  vacua, and the metastable and the true vacuum. We find that the typical velocity of the domain walls separating the two (degenerate) metastable vacua is 0.7 - 0.8, similar to that obtained in ref. [1] for  $b_1 = 0$  case. This is certainly expected. However, the velocity of domain wall separating the true vacuum and the metastable vacuum is found to be much larger in many cases, close to 1. Very accurate wall velocity estimates are not possible due to uncertainties in identifying wall location (with dynamically evolving wall profile). We show in Fig.6 and Fig.7 two different cases of 5 bubble nucleations (with different locations and phases inside the bubbles). Contour plots of energy density are shown in Fig.6a and 6b at  $\tau = 7.2$  and 7.8 fm (temperature at these stages is 208 and 201 MeV respectively). The portion of the domain wall near  $x = 14$  fm,  $y = 12$  fm in Fig.6a is seen to move towards left in Fig.6b with  $v \simeq 1$ . This is confirmed by the profile plot of  $l_0 - l$  in Figs.6c and 6d at same stages,  $\tau = 7.2$  and 7.8 fm respectively.

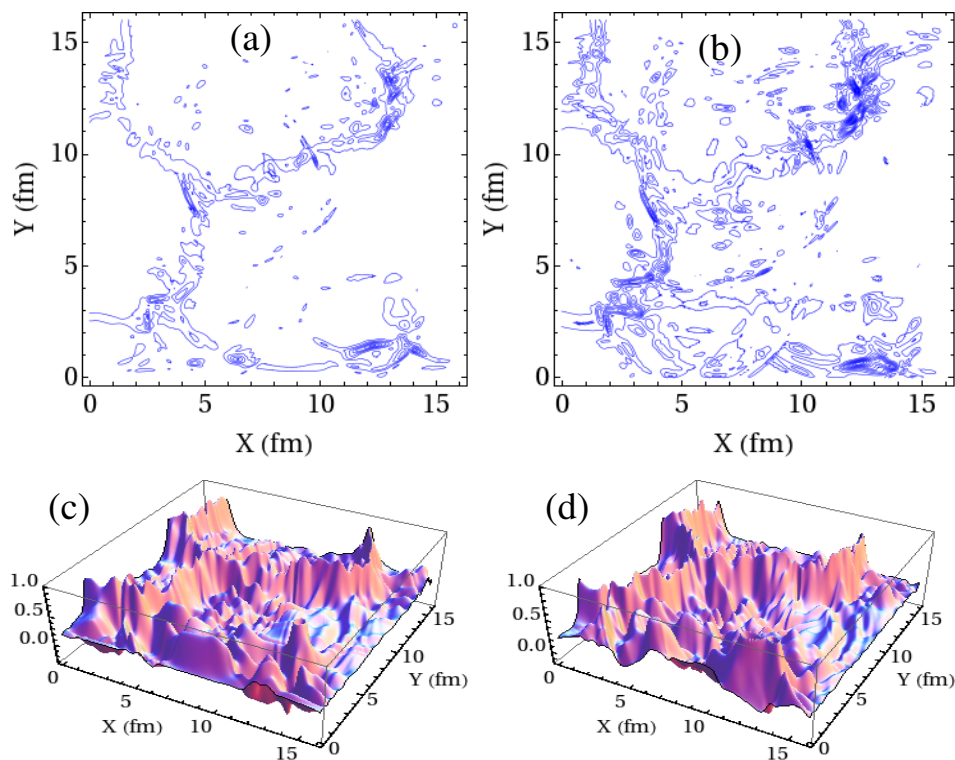


FIG. 6:

Contour plot of energy density at (a)  $\tau = 7.2$  fm and (b) at  $\tau = 7.8$  fm. Wall portion near  $x=14$  fm,  $y=12$  fm in (a) is seen to move towards left in (b) with large velocity. (c) and (d) show the profile plots of  $l_0 - l$  at these stages confirming the motion of the domain wall.

Fig.7 shows a different case of 5 bubble nucleation. (a) and (b) show the contour plots of energy density at  $\tau = 9.6$  and 10.9 fm. Temperature at these stages is  $T = 188$  and 180 MeV (note, this is slightly below  $T_c$ ). The location of wall in (a) is near  $x=9$  fm,  $y=8$  fm and this is seen to move towards lower right corner. This wall motion is confirmed by the profile plots of  $l_0 - l$  in Figs.7c,d.

### C. Rapid Collapse and Re-expansion

Perhaps the most dramatic difference between the present case with  $b_1 \neq 0$  and the previous case [1] of  $b_1 = 0$  is seen in Fig.8 and Fig.9. This shows the case of nucleation of 10 bubbles in a region of  $22$  fm  $\times$   $22$  fm. Though both of these numbers are somewhat large for RHICE, at least the size may not be too unrealistic for later stages of plasma evolution. Fig.8 shows a time sequence of the contour plot of energy density at  $\tau = 6.44, 8.20, 9.94, 11.34, 12.74,$  and  $14.5$  fm. The temperature at these stage is  $T = 215.0, 198.4, 186.0, 178.0, 171.2,$  and  $164.1$  MeV respectively.

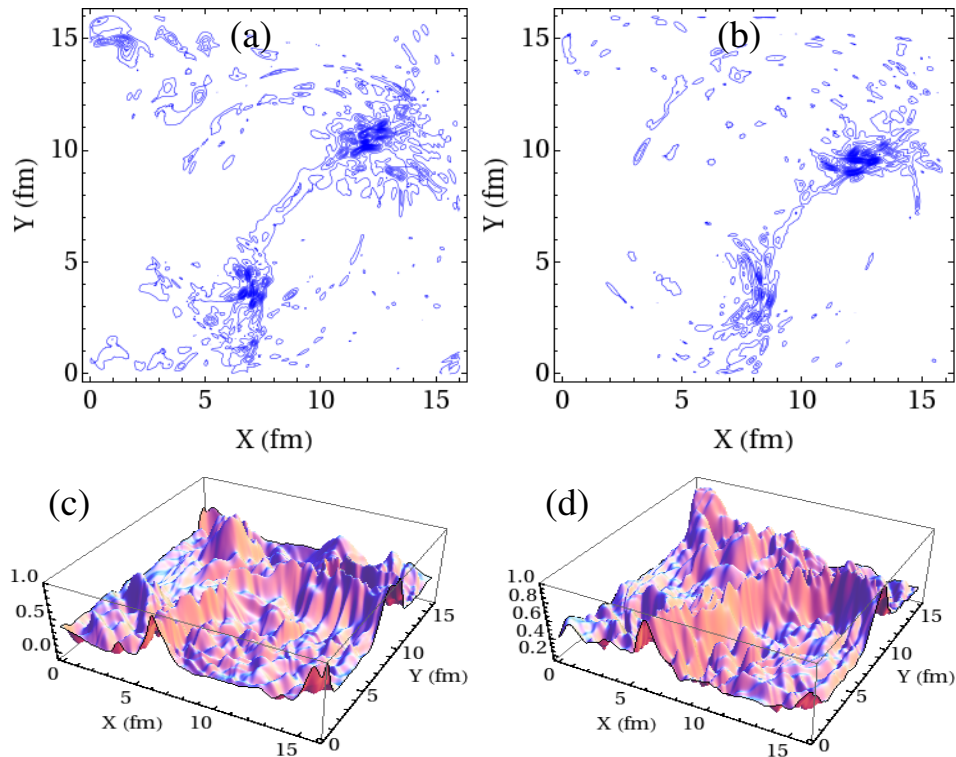


FIG. 7:

A different realization of 5 bubble nucleation. Contour plot of energy density at (a)  $\tau = 9.6$  fm and (b) at  $\tau = 10.9$  fm. Wall portion near  $x=9$  fm,  $y=8$  fm in (a) is seen to move towards lower right in (b) with large velocity. (c) and (d) show the profile plots of  $l_0 - l$  at these stages confirming the motion of the domain wall.

Note that  $T$  is below in (d) and after that. A closed domain wall is seen in the lower left region in (a) with  $x = 1-6$  fm and  $y = 5-11$  fm. This wall collapses rapidly by  $\tau = 9.94$  fm. The collapse velocity again is seen to be close to  $v \simeq 1$ . Interesting dynamics is seen for later plots when an expanding front is seen from the point of collapse. It rapidly expands, again with  $v \simeq 1$  all the way until last stages in (f). Presence of such an energetic expanding front is confirmed by the surface plots of energy density at the same stages as shown in Fig.9. Due to very large velocity and sharp profile of the expanding front it may well represent a shock front in the plasma.

## VII. POSSIBLE EXPERIMENTAL SIGNATURES OF Z(3) WALLS AND STRINGS WITH EXPLICIT SYMMETRY BREAKING

The  $Z(3)$  wall network and associated strings exist only during the QGP phase, melting away when the temperature drops below  $T_c$ . However, they may leave their signatures in the distribution of final particles due to large concentration of energy density in extended regions as well as due to non-trivial scatterings of quarks and antiquarks with these objects. The extended regions of high energy density resulting from the domain walls and strings are clearly seen in our simulations and some extended structures/hot spots also survive after the temperature drops below the transition temperature  $T_c$ . This is just as was seen in the case of  $b_1 = 0$  case in ref.[1]. We again mention that even the hot spot resulting from the collapse of closed domain walls in our simulations will be stretched in the longitudinal direction into an extended linear structure (resulting from the collapse of a cylindrical wall). These may be observable in the analysis of particle multiplicities. This is important especially in respect to the ridge phenomenon seen at RHIC [34]. In view of lasting extended energy density fluctuations from  $Z(3)$  walls, it is of interest to check if these structures can account for the ridge phenomenon.

Our results show interesting pattern of the evolution of the fluctuations in the energy density which show that these fluctuations do not decrease with time which was the case for  $b_1 = 0$  case studied in ref. [1]. Especially important may be the presence of small additional peak of short times for  $b_1 > 0$  case. Fluctuations near the transition stage may leave direct imprints on particle distributions. However, dileptons or direct photons should be sensitive to these

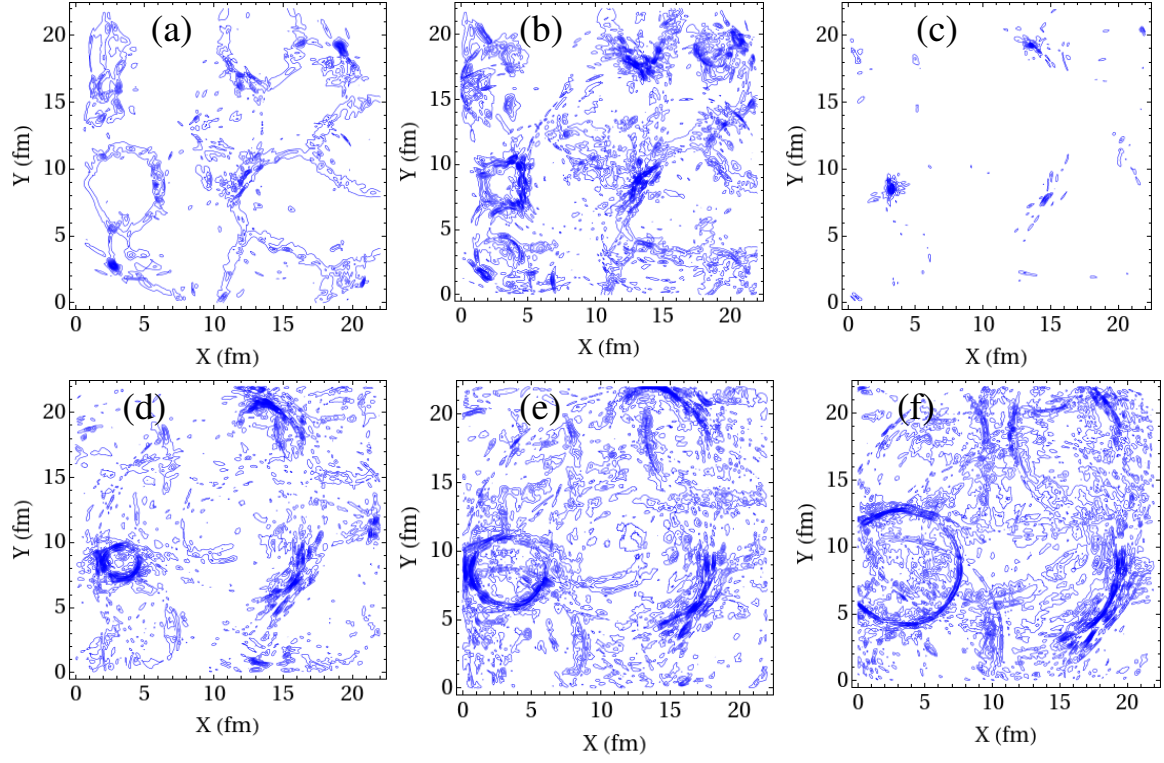


FIG. 8:

A case of 10 bubbles in  $22 \text{ fm} \times 22 \text{ fm}$  region. This figure shows a time sequence of contour plot of energy density showing rapid collapse of a domain wall (towards lower left) and subsequent rapid expansion of a circular front.

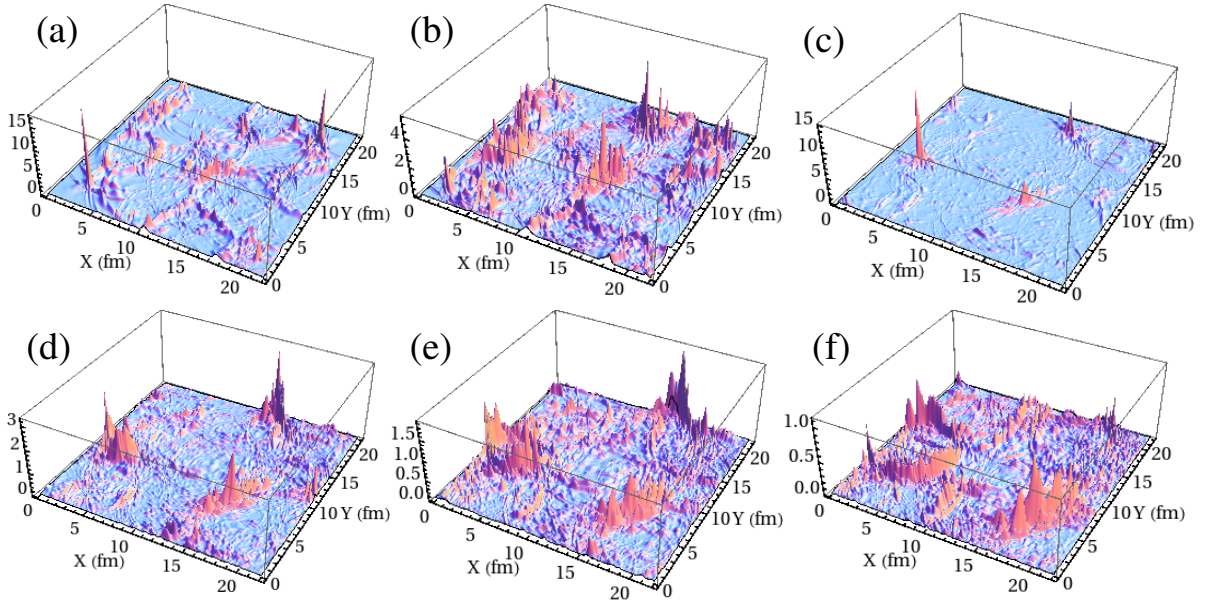


FIG. 9:

Surface plots of energy density for various stages shown in Fig.8

fluctuations, and these may give a time history of evolution of such energy density fluctuations during the early stages. In such a case the existence of small peak for  $b_1 > 0$  case may be observable.

A dramatic difference between the case of  $b_1 = 0$  and  $b_1 \neq 0$  is seen in Figs.8,9. Collapse of a closed wall is expected and was seen for  $b_1 = 0$  case also, though the wall speed here is much higher, close to 1. In general we have seen here that walls separating true vacuum from metastable vacuum have speeds much higher than seen for the case of  $b_1 = 0$ . What is qualitatively new in the present case is rapidly expanding circular front after the collapse of the wall. This front continues its speed and shape even when temperature drops below  $T_c$ . Possibility of such expanding circular (cylindrical, with longitudinal expansion) energetic fronts should have important implications on particle momenta, especially on various flow coefficients.

Another important difference due to  $b_1 > 0$  is expected in investigating the interactions of quarks and antiquarks with domain walls. Earlier we had argued [1] that collapsing  $Z(3)$  walls will lead to concentration of quarks (due to small non-zero chemical potential in RHICE) in small regions [3]. This will lead to enhancement of baryons, especially at high  $P_T$  [20] due to  $P_T$  enhancement of quarks/antiquarks as they undergo repeated reflections from a collapsing wall. (There is also a possibility of spontaneous CP violation in the scattering of quarks and antiquarks from  $Z(3)$  walls, see ref.[35].) However, with  $b_1 > 0$ , there may also be a possibility that some  $Z(3)$  wall may actually expand (the one enclosing the true vacuum and with sufficiently large size). In that case it will have opposite effect and baryon number will be more diffused. Even the enhancement of  $P_T$  may happen for some domain walls (those which enclose metastable vacuum) while the expanding closed walls (enclosing the true vacuum) should lead to the redshift of the momenta for the enclosed quarks. All these issues need to be explored with more elaborate simulations. In this context the difference in the wall velocity between different types of  $Z(3)$  walls is of importance. While studying the effects of quark reflections from these walls and associated modification of  $P_T$  spectrum, wall velocity is of crucial importance and the presence of different types of collapsing  $Z(3)$  walls may lead to bunches of hadrons with different patterns of modified  $P_T$  spectra.

## VIII. CONCLUSIONS

We have studied the effects of explicit symmetry breaking arising from quark effects on the formation and evolution of  $Z(3)$  interfaces and associated strings. Explicit symmetry breaking makes  $Z(3)$  vacua non-degenerate with two vacua  $l = z, z^2$  remaining degenerate with each other but having higher energy than the true  $l = 1$  vacuum. Thus  $l = z, z^2$  vacua become metastable. We have used an effective potential for the Polyakov loop expectation value  $l(x)$  from ref. [9, 10] with incorporation of explicit symmetry breaking in terms of a linear term in  $l$  and have studied the dynamics of the (C-D) phase transition in the temperature/time range when the first order transition of this model proceeds via bubble nucleation. This allows for only relatively small explicit symmetry breaking (characterized by the strength  $b_1$  of the linear term in  $l$ ). We again emphasize that, though our study is in the context of a first order transition, its results are expected to be valid even when the transition is a cross-over. This is because our focus is only on the formation of topological objects whose formation (via Kibble mechanism) only depends on the formation of a domain structure and not crucially on the dynamics of the phase transition. Though, our statements about the energetics of bubble walls etc. clearly apply only for a first order transition.

An important result we have discussed in this paper relates to expected relative importance of the metastable  $Z(3)$  vacua. Due to higher energy of these vacua one would expect that bubbles with these vacua should form with relatively lower probability (even with small values of  $b_1$  we have used). However, we find interesting results due to nontrivial interplay of the pre-exponential factor and the exponential term in the nucleation rate for the bubbles. While the exponential term leads to a decrease in the rate for metastable vacua due to larger action, the pre-exponential factor leads to an increase in the rate for larger action. For a suitable range of temperatures, which for our choice of parameter values lies between  $T = 200$  MeV to  $T = 225$  MeV, the metastable vacuum bubbles have the same or larger nucleation rate compared to the true vacuum bubbles. As the metastable vacuum bubbles also have larger sizes it means that a larger fraction of QGP phase may get converted to the metastable  $Z(3)$  vacua than to the true  $Z(3)$  vacuum. The dynamics of these domains being so different its effects on the evolution of plasma and various signals may be important.

## Acknowledgments

We are very grateful to Sanatan Digal, Anjishnu Sarkar, Ananta P. Mishra, P.S. Saumia, and Abhishek Atreya for very useful comments and suggestions. USG, AMS, and VKT acknowledge the support of the Department of Atomic Energy- Board of Research in Nuclear Sciences (DAE-BRNS), India, under the research grant no 2008/37/13/BRNS.



USG and VKT acknowledge support of the computing facility developed by the Nuclear-Particle Physics group of Physics Department, Allahabad University under the Center of Advanced Studies (CAS) funding of UGC, India.

- 
- [1] U. S. Gupta, R. K. Mohapatra, A. M. Srivastava and V. K. Tiwari, Phys. Rev. **D82**, 074020 (2010).  
 [2] B. Layek, A.P. Mishra, A.M. Srivastava, Phys. Rev. **D 71**, 074015 (2005).  
 [3] B. Layek, A.P. Mishra, A.M. Srivastava, and V.K. Tiwari, Phys. Rev. **D 73**, 103514 (2006).  
 [4] L.D. McLerran and B. Svetitsky, Phys. Rev. **D24**, 450 (1981); B. Svetitsky, Phys. Rept. **132**,1 (1986).  
 [5] T. Bhattacharya, A. Gocksch, C. K. Altes, and R. D. Pisarski, Nucl. Phys. **B 383**, 497 (1992); J. Boorstein and D. Kutasov, Phys. Rev. **D 51**, 7111 (1995).  
 [6] A. V. Smilga, Ann. Phys. **234**, 1 (1994).  
 [7] V.M. Belyaev, Ian I. Kogan, G.W. Semenoff, and N. Weiss, Phys. Lett. **B277**, 331 (1992).  
 [8] C.P. Korthals Altes, hep-th/9402028  
 [9] R.D. Pisarski, Phys. Rev. **D62**, 111501R (2000); *ibid*, hep-ph/0101168.  
 [10] A. Dumitru and R.D. Pisarski, Phys. Lett. **B 504**, 282 (2001); Phys. Rev. **D 66**, 096003 (2002); Nucl. Phys. **A698**, 444 (2002).  
 [11] M. Deka, S. Digal, and A.P. Mishra, arXiv:1009.0739.  
 [12] A. Dumitru, D. Roder, and J. Ruppert, Phys. Rev. **D70**, 074001 (2004).  
 [13] T. Banks and A. Ukawa, Nucl. Phys. **B225** 145 (1983).  
 [14] F. Green and F. Karsch Nucl. Phys. **B238** 297 (1984).  
 [15] P. N. Meisinger and M. C. Ogilvie, Phys. Rev. **D 52**, 3024 (1995).  
 [16] S. Digal, E. laermann, and H. Satz, Nucl. Phys. **A 702**, 159c (2002); F. Karsch, E. Laermann, A. Peikert, Ch. Schmidt, and S. Stickan, Nucl. Phys. **B 94** (Proc. Suppl.) 411 (2001).  
 [17] J. Ignatius, K. Kajantie, and K. Rummukainen, Phys. Rev. Lett. **68**, 737 (1992); V. Dixit and M.C. Ogilvie, Phys. Lett. **B 269**, 353 (1991).  
 [18] T.W.B. Kibble, J. Phys. **A 9**, 1387 (1976); Phys. Rep. **67**, 183 (1980);  
 [19] W.H. Zurek, Phys. Rep. **276**, 177 (1996).  
 [20] A.P. Mishra, A.M. Srivastava, and V.K. Tiwari, Ind. J. Phys. **85**, 1161 (2011).  
 [21] A. Bazavov, B.A. Berg, and A. Dumitru, Phys. Rev. **D78**, 034024 (2008).  
 [22] K. Fukushima, Phys. Lett. **B591** 277 (2004), arXiv:hep-ph/031012; S. Rosner, C. Ratti, and W. Weise, Phys. Rev. **D75** 034007 (2007), arXiv: hep-ph/0609281; D. Diakonov and M. Oswald, hep-ph/0403108  
 [23] O. Scavenius, A. Dumitru and J.T. Lenaghan, Phys. Rev. **C66**, 034903 (2002).  
 [24] G. Boyd, J. Engels, F. Karsch, E. Laermann, C. Legeland, M. Lutgemeier, and B. Petersson, Nucl. Phys. **B469**, 419 (1996); M. Okamoto et al., Phys. Rev. **D60**, 094510 (1999).  
 [25] S. Chang, C. Hagmann, and P. Sikivie, Phys. Rev. **D59**, 023505 (1999); M.C. Huang and P. Sikivie, Phys. Rev. **D32**, 1560 (1985).  
 [26] S. Digal and A.M. Srivastava, Phys. Rev. Lett. **76** 583 (1996); S. Digal, S. Sengupta, and A.M. Srivastava, Phys. Rev. **D55** 3824 (1997).  
 [27] M.B. Voloshin, I.Yu. Kobzarev, and L.B. Okun, Yad. Fiz. **20**, 1229 (1974) [Sov. J. Nucl. Phys. **20**, 644 (1975)]; S. Coleman, Phys. Rev. **D15**, 2929 (1977).  
 [28] A.D. Linde Nucl. Phys. **B216**, 421 (1983).  
 [29] J. S. Langer, Ann. Phys. (N. Y.) **54**, 258 (1969); J. S. Langer and L. A. Turski, Phys. Rev. **A 8**, 3230, (1973); L. A. Turski and J. S. Langer, Phys. Rev. **A 22**, 2189 (1980)  
 [30] L. P. Csernai and J. I. Kapusta, Phys. Rev. **D 46**, 1379 (1992); J.I. Kapusta, A.P. Vischer, and R. Venugopalan, Phys. Rev. **C 51**, 901 (1995)  
 [31] J.D. Bjorken, Phys. Rev. **D 27**, 140 (1983).  
 [32] A.M. Srivastava Phys. Rev. **D45**, R3304 (1992); Phys. Rev. **D 46**, 1353 (1992); S. Chakravarty A.M. Srivastava Nucl. Phys. **B406**,795 (1993).  
 [33] T.C. Petersen and J. Randrup, Phys. Rev. **C 61**, 024906 (2000).  
 [34] J. Adams et al. [STAR Collaboration], J. Phys. **G 32**, L37,(2006) [arXiv:nucl-ex/0509030]; J.Putschke, Talk at Quark Matter 2006 for STAR collaboration), Shanghai, Nov.2006; S. A. Voloshin, Phys. Lett. **B 632**, 490 (2006)[arXiv:nucl-th/0312065]; A. Dumitru, F. Gelis, L. McLerran, and R. Venugopalan, Nucl. Phys. **A 810**, 91 (2008).  
 [35] A. Atreya, A. Sarkar, and A.M. Srivastava, arXiv:1111.3027